European Journal of Mechanics B/Fluids 28 (2009) 506–520

Contents lists available at ScienceDirect

European Journal of Mechanics B/Fluids

www.elsevier.com/locate/ejmflu

Analytical solutions for a single blade in vertical axis turbine motion in two-dimensions

P. Deglaire [a], S. Engblom [b], O. Ågren [a,*], H. Bernhoff [a]

[a] Uppsala University, The Ångström Laboratory, Swedish Centre for Renewable Energy Conversion, Division for Electricity and Lightning Research, Department of Engineering Sciences, Box 534, SE-751 21 Uppsala, Sweden
[b] Department of Information Technology, Scientific Computing, Box 337, SE-751 05 Uppsala, Sweden

ARTICLE INFO

Article history:
Received 4 February 2008
Received in revised form 4 October 2008
Accepted 25 November 2008
Available online 3 December 2008

Keywords:
Vertical axis turbine
Conformal mapping
Vortex method
Rotating wing
Laurent's series
Fast Multipole Method

ABSTRACT

An analytical model for a time dependent two dimensional flow around a moving profile is developed. The model is suitable for fast aerodynamic and aeroelastic coupling calculations. It determines the inviscid pressure distribution in the vicinity of one blade and the force on the blade in arbitrary two dimensional motion. The method is more flexible than previous analysis: it can represent any profile, pitching motion and blade attachment position. The method is based on conformal mapping techniques and Laurent's series decomposition and is faster and more accurate than standard panel methods. A main idea is to directly treat the singularities of the flow in a mapped plane where any geometrical plane is simplified to a circle. The vorticity is assumed to be shed in the form of a continuous vortex sheet near the trailing edge.

© 2008 Elsevier Masson SAS. All rights reserved.

1. Introduction

The turbine in the present investigation has a vertical shaft connected to straight vertical blades via support beams instead of the horizontal shaft used in conventional wind turbines (see Fig. 1).

The vertical axis wind turbine concept was invented by J.M. Darrieus [1] in 1931, and a renewed interest for the concept appeared during the oil crisis in the 1970's.

The vertical axis wind turbines (or VAWT) are again considered for large and small scale wind power generation, see Fig. 1. They can also be used to produce energy from underwater currents. At Uppsala University, the main focus is on simple turbine construction to minimize costs [2]. The effort includes the usage of improved composite materials, wind turbine aerodynamics and new generations of permanent magnet high voltage generators that avoid mechanical gears. However, in particular two key issues need to be resolved.

Firstly, the vertical axis turbines experience a complicated flow with remaining theoretical uncertainties. An efficient tool had not been previously developed for a systematic theoretical design study of the pitch angle, attachment point and shape of the blades. In most experimental and theoretical studies the old NACA 4 digit series airfoil has been used [3].

Secondly, the structural design of the turbine is demanding. Hence, without the use of special composites materials and accurate models it is difficult to build a reliable turbine [4]. This could be a major reason why the worldwide research efforts on vertical axis turbines have declined for the last two decades. Most of the previous vertical axis program stopped due to failures of a blade or the main bearing. After the damage of the world's largest vertical axis turbine in the 1990's, the 3.2 MW rated power Eole in Cap Chat at Quebec [4], almost all large scale Darrieus and H-rotor research projects have been stopped.

It is commonly believed that vertical turbines are much less efficient than their horizontal counter parts. However, it should be kept in mind that commercial horizontal wind turbines have been optimized for more than twenty years. For instance, the reported maximum measured power coefficient [5] of the VAWT 260 in Great Britain is as high as 0.39, which twenty years ago was an acceptable figure of merit. Substantial progress could be expected if the understanding of the physics of vertical turbines would be deepened.

The design of the turbine can be improved, for instance by minimizing the drag produced by struts and junctions. Their special aerodynamic features such as vortex shedding may turn out to be advantageous for small and medium size electricity production from wind or underwater streams (vortex shedding is used by insects and fish to produce a very powerful thrust [6]). Finally, the overall design could be simplified and thus be made more cost efficient.

* Corresponding author. Tel.: +46 18 471 58 16; fax: +46 18 471 3000.
E-mail address: Olov.Agren@Angstrom.uu.se (O. Ågren).

0997-7546/$ – see front matter © 2008 Elsevier Masson SAS. All rights reserved.
doi:10.1016/j.euromechflu.2008.11.004

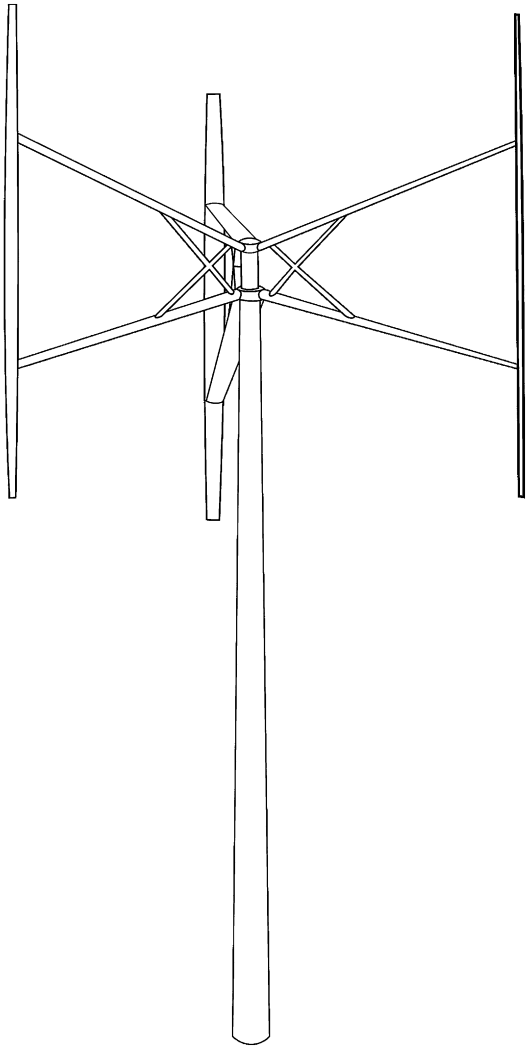

Fig. 1. General view of an H-rotor with three blades.

2. Previous aerodynamic models

The methodology described in this paper has been developed with emphasis on two peculiarities of cross flow turbines: the complicated flow surrounding vertical turbines and the sensitive dependency on various aerodynamic parameters. Features that need to be investigated in more detail are: the unsteady interaction between the blades due to the continuously changing angle of attack via vortex shedding and unsteady relative flow curvature seen by the blades during rotation [7]. Additionally, the wing profile affects strongly the dynamic stall performance. Some of these effects may be studied more efficiently with the method described here.

Previously, vertical axis turbines have been modeled in three ways: (i) a streamtube analysis (also called blade element momentum theory) [3,8] originating from the horizontal axis turbines theory, (ii) vortex models [9–12] and (iii) Computational Fluid Dynamics (CFD) models [13–15]. The third group of models may be more accurate and reliable, but is more demanding in terms of computing effort and time as compared to the others. The two first models typically need inputs in the form of lift and drag data as determined from computations or experiments. In most cases this set of data is taken from non moving wind tunnel experiments or steady state calculations. As the local flow conditions are radically different, the results from such static tests cannot be considered. Moreover, the static data needs to be related to the fully interactive flow encountered by the wings. This is usually done by calculating the relative angle of attack seen by the blade in motion. However, even the definition of this effective angle of attack may be questionable in view of the complicated flow experienced by real vertical turbine blades. A simple analytical model is presented in this paper to clear these uncertainties concerning two of the aforementioned aspects: flow curvature influence and blade–wake interaction.

The present work has been inspired by three previous studies. One of the most complete models for vertical axis turbines is a vortex model developed by Oler and Strickland [9], but it disregards flow curvature. The use of the panel method complicates the vortex shedding treatment and increases the computational cost. The panel method, however, can be generalized to three dimensions unlike methods based on conformal mapping.

The analytic study of Wilson [10] uses the conformal mapping from a flat plate to a circle via the Joukowsky transform. The advantage of his study is the analytical simplicity. However, the flat plate is not a suitable airfoil for vertical axis turbines (it has not a preferential direction of rotation) and generalizations are necessary. Another study was carried out by Zervos et al. [16] using the results of Couchet [17] for the aerodynamics of arbitrary two dimensional profiles in general two dimensional motion. It was applied to a NACA0012 airfoil but the oversimplified computation [16] did not give convincing results.

Zannetti [18] recently applied a discrete vortex model to study vortex trapping blades for vertical axis turbines. However, the forces on the blades were not evaluated. Moreover it does not seem straightforward to apply that model to N bladed turbines or N boundary problems. The computation time in the present paper is reduced by using a suitable implementation of the Fast Multipole Method (FMM) algorithm [19]. Wang [12], also recently applied a 2D panel-method to the simulation of the flow around a multi-bladed conventional VAWT.

The model presented in this paper is a generalization of Wilson's [10] vortex model to an arbitrary profile in arbitrary motion. Therefore the model will inherit the flexibility of Oler's [9] model and benefit from exact calculations to decrease significantly the computing time. The generalization to the N bladed case has been investigated by Österberg [20]. The present model is able to determine the inviscid pressure distribution on the rotating blade. Some possible future developments of this analysis (influence of viscosity and aeroelastic computations) are not developed here but briefly given in Section 8 as perspectives.

The model is presented in several steps. Firstly, the geometry of the physical problem is defined and simplified via conformal mapping techniques. The set of equations to be solved together with the appropriate boundary conditions are established and solution details are given. Exact formulas for the forces from the fluid on the blades are also derived. Explicit results are presented for an application to vertical axis turbine flows.

3. Geometry definition, Laurent's series and conformal maps

A conformal mapping is a transformation which preserves local angles in the transformation. Riemann [21] showed that there exists a conformal map which transforms the exterior of any shape (here an airfoil) onto the exterior of the unit disk. The conformal mapping transformation is analytic. It follows that there exists a Laurent series expansion of this transform which enables a fast evaluation of the mapping [22] and simplifies the treatment of derivatives and integrations over the airfoil contour.

The airfoil coordinates are given by a set of discrete coordinates (x_{Ci}, y_{Ci}) converted into a set of complex numbers $z_{Ci} = x_{Ci} + iy_{Ci}$.

The conformal transformation f is considered in the form of a Laurent' series:

$$z = f(s) = s + \sigma + \sum_{k=1}^{+\infty} \frac{c_k}{s^k} b^k, \tag{1}$$

where σ and c_k are complex numbers. The function f transforms a circle s_c of radius b in the s-plane into the wing section z_c in the z-plane, represented by a discrete set of points.

$$s_c = be^{i(\eta+\eta_{TE})}, \tag{2}$$

where η_{TE} is the trailing edge angle in the transformed plane.

The aim is to find the optimal σ and $\{c_n\}_{n\in N}$ that approaches as closely as possible the shape given by interpolation of the points z_i of the airfoil section.

The method used here is based on Ives' [23] FFT method and adapted to obtain the Laurent's series coefficients as described by Deglaire [22]. The airfoil shape resulting from applying the transformation offers a precision of four digits and the computational time required to carry out this process is on the order of milliseconds on a personal computer.

The area of the section A and its center ζ can be calculated analytically if the conformal transformation is known.

The general transformation is defined by Eq. (1). Specializing to the case of the vertical axis turbine, four new parameters are introduced: the rotor radius $a(t)$, the pitch angle $\delta(t)$, the blade shift position $x_0(t)$ and the angular position of the blade at time t, $\beta(t)$ (see Fig. 2). All these four parameters are allowed to change in time. Additional to the coordinate system defined by z, three coordinate systems z_1, z_2, z_3 are defined as follows:

$$z_1 = (z + x_0)e^{-i\delta}, \tag{3}$$

$$z_2 = z_1 + ia, \tag{4}$$

$$z_3 = z_2 e^{i\beta}, \tag{5}$$

which represent rigid displacement and rigid rotations of the foil.

A possible implementation of this theory is to study the effects of small pitch and heave oscillations superimposed on the usual rotation corresponding to the β angle to investigate aeroelastic instabilities. The rotations including the β and the δ angle could have been reduced to one rotation. However, it was decided for convenience to keep this "double" rotation formalism.

The z coordinates represents the position of the points fixed to the foil and the coordinates z_3 the points seen by an observer fixed in the earth frame and looking to the turbine from above. A point attached to the z frame is moving in the z_3 frame with the velocity

$$V_{z/z3inz3} = i\dot{\beta}z_3 + \dot{x}_0 e^{-i(\delta-\beta)} - i\dot{\delta}z_1 e^{i\beta} + i\dot{a}e^{i\beta} \tag{6}$$

expressed in the z_3 frame coordinates. This is noted using the subscript $z/z3inz3$.

4. Equations and boundary conditions

Under the assumption of incompressible and inviscid flow written in the (assumed) inertial earth frame (or the lab frame), we obtain for the velocity $\vec{V}_3$ in this z_3-inertial frame:

$$\vec{\nabla} \cdot \vec{V}_3 = 0, \tag{7}$$

and adding the extra condition of irrotational flow in the lab:

$$\vec{\nabla} \times \vec{V}_3 = 0. \tag{8}$$

Thus introducing two potential function φ and ψ which respectively are the velocity potential and the stream function, satisfying Laplace's equation and the Cauchy–Riemann relations [24].

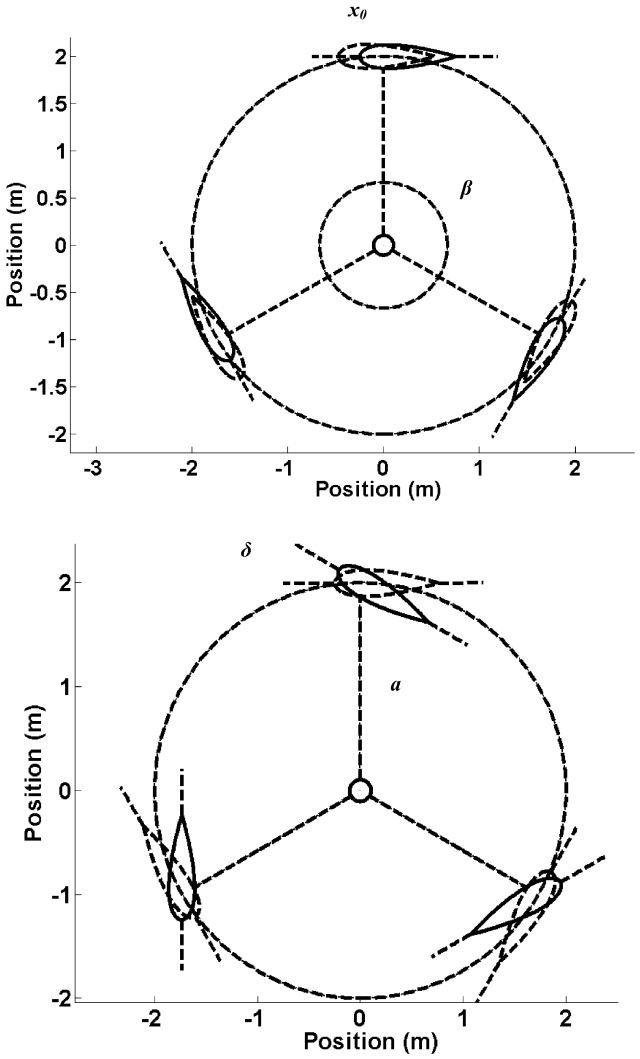

Fig. 2. Definition of the main parameters in the H rotor section.

A complex potential is introduced

$$F = \varphi + i\psi, \tag{9}$$

such that

$$V_3 = \overline{\frac{dF}{dz_3}}, \tag{10}$$

where the bar symbol represents complex conjugate. Any function F which is an analytic function is a solution to this problem.

This problem is subjected to three boundary conditions. A first boundary condition states that the velocity should coincide with the wind velocity at infinity. A second boundary condition states that the fluid should not penetrate inside the wing in the non-inertial z frame. An extra boundary condition analog to the Kutta–Joukowsky condition will be introduced by stating that the velocity in the non-inertial frame should be exactly zero at the trailing edge.

Hence a complex potential which is an analytical function and fulfills the following three boundary conditions:

$$\frac{dF}{ds} \underset{s\to\infty}{\longrightarrow} V_0 e^{i(-\alpha+\beta-\delta)}, \tag{11}$$

$$F(s) - \bar{F}(\bar{s}) - 2i\psi_3(s,\bar{s}) = iK, \quad \text{for } s\bar{s} = b^2, \tag{12}$$

$$\frac{dF}{dz_3} - \bar{V}_{z/z3inz3} = 0 \quad \text{for } s = be^{i\eta_{TE}} \tag{13}$$

is a solution to the problem. In Eq. (11), V_0 is the norm of the wind speed and α is the angle between the wind velocity and the real axis. Eq. (12) is expressed for all points in a circle which are mapped to the foil. K is real valued and the stream function ψ_3 is representing the blade in vertical axis motion by

$$\psi_3(s,\bar{s}) = -\frac{1}{2}\dot{\beta} z_3 \bar{z}_3 + \frac{1}{2}\dot{\delta} z_1 \bar{z}_1 + \mathrm{Im}(-i\dot{a} z_1 + \dot{x}_0 z). \tag{14}$$

5. Solution

5.1. Complex potential

Regarding the form of Eqs. (9), (11) and Eq. (12), (13), it seems appropriate to look for an *F(s)* in the form of an analytic function and express it in the form of a Laurent's series similarly to the airfoil transform. Thus, considering the asymptotic behavior of F at infinity up to a constant:

$$F(s) = V_0 e^{i(-\alpha+\beta-\delta)} s + V_0 e^{-i(-\alpha+\beta-\delta)} \frac{b^2}{s} + \sum_{\nu=1}^{N_v} \left[\frac{i\Gamma_\nu}{2\pi} \left(\log(s - s_\nu) - \log\left(s - \frac{b^2}{\bar{s}_\nu} \right) \right) \right] + F_1(s), \tag{15}$$

where Γ_ν are the strengths of the wake vortices and their images. These Γ_ν are primarily a consequence of the unsteady motion of the wing (technically the Kutta condition at the trailing edge). At each step one trailing vortex with a given strength is created and then shed. The set of these trailing vortices forms the wake of the foil and of the turbine.

The function F_1 is given as

$$F_1 = \sum_{k=1}^{\infty} \frac{G_k}{s^k} b^k, \tag{16}$$

where

$$G_k = -i\dot{\beta} G_{A,k} + i\dot{\delta} G_{B,k} - i\dot{a} G_{C,k} + \dot{x}_0 G_{D,k}. \tag{17}$$

All coefficients $\{G_k\}_{k\geqslant 1}$ can be derived analytically by straightforward identifications from the non-penetration boundary condition and the coefficients can be found in Appendix A. The complex potential F is now totally determined and corresponds to the exact solution of Laplace's equation for an arbitrary boundary in arbitrary two dimensional motion. The streamlines in the z plane can be found by determining the isovalues of the function

$$\psi_r = \mathrm{Im}(F) - \psi_3. \tag{18}$$

5.2. Velocity field

Knowing the complex potential F, the "absolute" velocity is derived in the z-plane as

$$V_z = \frac{\overline{dF}}{\overline{dz}} = \frac{\overline{dF}}{\overline{ds}} \frac{\overline{ds}}{\overline{dz}}, \tag{19}$$

and the absolute velocity in the z_3 frame is derived as

$$V_3 = \frac{\overline{dF}}{\overline{dz_3}} = V_z \frac{\overline{dz}}{\overline{dz_3}}. \tag{20}$$

The relative velocity expressed in the z_3 frame for a point fixed to the foil (attached to the z frame) is then

$$V_{R3} = V_3 - V_{z/z3inz3}. \tag{21}$$

5.3. Kutta condition

The Kutta condition is satisfied at each time step by locating a new vortex at the trailing edge of the profile in the way described by Streitlien [25]. The strength of this vortex is determined using the Kutta–Joukowsky condition described in Eq. (13).

$$\frac{dF}{dz_3} - \bar{V}_{z/z3inz3} = 0, \tag{22}$$

at the trailing edge point $s = be^{i\eta_{\mathrm{TE}}}$.

Assuming that $N_V - 1$ vortices are present in the flow from the $N_V - 1$ previous time steps, let s_{N_v} be the position of the newly emitted vortex in the s plane and s_{TE} the position of the trailing edge. It is now possible to determine the unknown nascent circulation by

$$\left.\frac{dF}{ds}\right|_{s_{\mathrm{TE}}} = \bar{V}_{z/z3inz} \left.\frac{dz}{ds}\right|_{s_{\mathrm{TE}}}. \tag{23}$$

5.4. Numerical implementation

All the created vortices are advanced in time according to the absolute velocity of the fluid. At each vortex location the convection velocity is corrected using Routh's rule [26]. The update of the vortex positions in the circle plane can be carried out following the direct procedure of Österberg [20] or the inverse mapping procedure of Deglaire [22]. Under the inviscid assumption the strength of all vortices is kept constant once they are ejected. The computationally expensive convection of the vortices is carried out using the Fast Multipole Method and the images are automatically taken care of via the fast imaging method developed by Deglaire [22].

The fast multipole method (FMM) was first described in Greengard and Rokhlin's famous 1987 paper [27] and was subsequently improved by incorporating adaptivity [18], fast translation operators [28] and improved implementation in 3D [29,30].

The fundamental idea, however, remains the same: far away from a point source, the potential becomes smooth and can be well approximated by a few terms in a rapidly convergent series – the potential is of low effective *rank*. It follows that the effect of potentials at a large enough distance, belonging to a set which is *well separated* from the set of points of interest, can be accurately computed as a set-to-set interaction rather than as an expensive particle-to-particle interaction.

The N potentials are sorted into boxes that are hierarchically ordered in a tree. At each level in the tree, clusters of particles that are neighbors interact in such a way that the low-rank (and hence effective) representation is used whenever possible. Direct interaction between particles is only allowed at the very finest level in the tree resulting in an algorithm with running time proportional to the number of particles N.

An *adaptive* implementation improves this for non-uniform distributions of particles by only refining the tree were needed. Other improvements focus on the complexity constant by optimizing the implementation of the translation operators. A straightforward implementation runs in time proportional to $O(p^2)$ in 2D and $O(p^4)$ in 3D, where $p \approx -\log_2(tol)$ is the number of expansion terms and *tol* is the numerical tolerance. In the latest generation of FMMs, these estimates can be brought down to $O(p\log(p))$ in 2D [28] and to $O(p^2)$ in 3D [30].

Since vortex methods take place in 2 space dimensions we have focused our implementation of the FMM to 2D. A neat scheme which avoids the traditional tree implementation was devised in [31]. At medium accuracy, the gain in using the asymptotically effective implementation of the translational operators is offset by large constants and a complicated implementation in order to

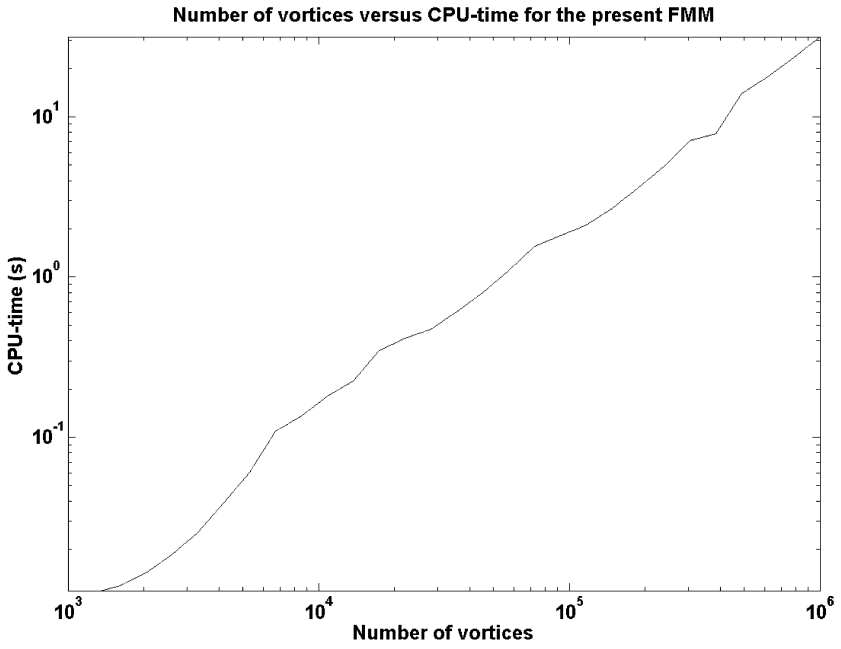

Fig. 3. Number of vortices vs. CPU-time in seconds for our implementation of the fast multipole method.

guarantee numerical stability. Instead, we have focused on making the constant in front of $O(p^2)$ as small as possible. This can be achieved on a vast amount of computer architectures by the use of BLAS routines [32]. By a novel version of the direct addressing implementation in [31], data is not only localized in the sense that nodes that interact are located closely in memory, but also *aligned* so that large blocks of coefficients can interact simultaneously through BLAS level-3 calls. In this fashion, an efficient implementation emerges (see Fig. 3). These results were obtained on a single processor 2.6 GHz computer.

Another feature of our implementation is a Mex-interface to Matlab which makes it possible to code and experiment with the vortex method. The FMM-code is available in [33].

6. Pressure distribution on the moving blades

To find the forces from the pressure acting on the foil, the unsteady Bernoulli equation in the form of Couchet [17] is written in terms of variables expressed in the moving z-plane but the velocity is the absolute velocity from Eq. (20).

In the z_3 frame,

$$\frac{p}{\rho} = -\frac{1}{2}\left(|V_3|\right)^2 - \frac{\partial\varphi(z_3,\bar{z}_3,t)}{\partial t} + C(t). \tag{24}$$

Omitting the time dependent constant, the pressure is therefore

$$\frac{p-p_\infty}{\rho} = -\frac{1}{2}\left(|V_3|\right)^2 - \frac{\partial\varphi(s,\bar{s},t)}{\partial t} + \mathrm{Re}[V_3\bar{V}_{z/z3inz3}]. \tag{25}$$

Pressure coefficients can be introduced as in Oler [8] by

$$C_P = \frac{p-p_\infty}{1/2\rho V_b^2}, \tag{26}$$

where

$$V_b = \left|V_0 e^{i\alpha} - V_{z/z3inz3}(z_{3c})\right|, \tag{27}$$

and z_{3c} is chosen to be the attachment point.

The present model neglects viscous effects, which is especially important in the analysis of kW rated Darrieus turbines. If integrated, the obtained pressure distribution will give rise to normal and tangential forces which are too high compared to the experimental values and only valid for low angles of attack. Although not complete this pressure distribution can be used to explain some basic features of VAWT operation.

7. Force calculations

We can now express the elemental force due to the pressure from the fluid on the blade via the complex number

$$dN = ip\,dz. \tag{28}$$

The inviscid pressure forces can be integrated numerically and are given in the z frame by

$$X - iY = -\oint_C ip\,d\overline{z}, \tag{29}$$

where C is the airfoil contour in the z plane. The pitching moment with respect to the origin of the z plane is

$$M_0 = \mathrm{Re}\left[\oint_C pz\,d\overline{z}\right]. \tag{30}$$

In the present work the final analytical formulas for the pitching moment calculations are not presented. However, with the use of the extended Blasius formula [34] and the residue theorem the analytical calculation can be carried out [25].

The forces can be integrated analytically (for details see Appendix B). It is found that

$$X - iY = \frac{i\rho}{2}[E + I], \tag{31}$$

with

$$\begin{aligned} E = {} & -2\left(2(\dot{\beta}-\dot{\delta})\pi\left(V_0 e^{i(-\alpha+\beta-\delta)}b^2 + \bar{G}_1 b - V_0 e^{-i(-\alpha+\beta-\delta)}\bar{c}_1 b\right)\right) \\ & - 2(\dot{\beta}-\dot{\delta})\bar{V}_{z/z3inz0}A + i(\dot{\beta}-\dot{\delta})^2\frac{4A}{3}\bar{\zeta} - \frac{4A}{3}\bar{\zeta}[\ddot{\delta}-\ddot{\beta}] \\ & - 2iAA_{z/z3inz} + 4i\pi b\left(\bar{c}_1\left[\frac{\partial V_0}{\partial t}e^{-i(-\alpha+\beta-\delta)}\right.\right. \\ & \left.\left. - V_0 i(-\dot{\alpha}+\dot{\beta}-\dot{\delta})e^{-i(-\alpha+\beta-\delta)}\right] - \bar{D}_1\right), \end{aligned} \tag{32}$$

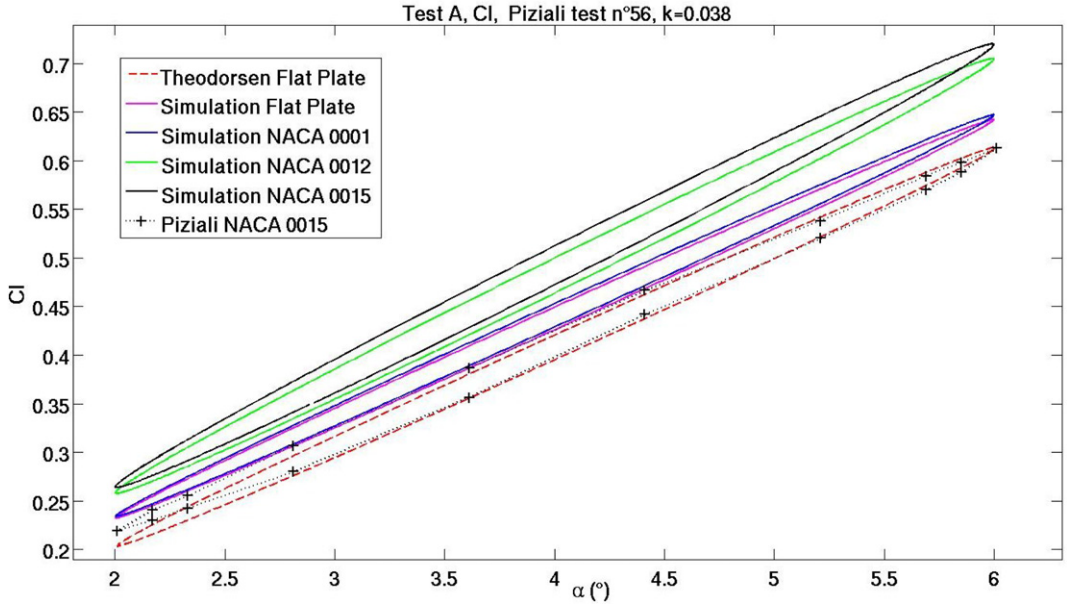

Fig. 4. Lift coefficient vs. pitch angle for different profiles in sinusoidal pitching motion with a low reduced frequency of 0.038 from 2 to 6 degrees. (For interpretation of the references to colour in this figure legend, the reader is referred to the web version of this article.)

where A is the area of the profile, ζ the complex position of the center of moment and $V_{z/z3inz0}$, $A_{z/z3inz}$ and D_1 are given in Appendix B.

$$I = 2\sum_{v=1}^{N_v}\Gamma_v\frac{d\bar{z}_v}{dt} - 2\bar{V}_{entz0}\sum_{v=1}^{N_v}\Gamma_v + 2i(\dot{\beta}-\dot{\delta})\sum_{v=1}^{N_v}\Gamma_v\left[\bar{z}_v - \bar{s}_v + \frac{b^2}{s_v}\right] - 2\sum_{v=1}^{N_v}\Gamma_v\left(\frac{\partial\bar{s}_v}{\partial t}\frac{d\bar{z}_v}{d\bar{s}_v} - \frac{\partial\bar{s}_v}{\partial t} + \frac{\partial}{\partial t}\left(\frac{b^2}{s_v}\right)\right). \quad (33)$$

To include the nascent vortices this last formula is rephrased as

$$I \cong -2i(\dot{\beta}-\dot{\delta})\sum_{v=1}^{N_v}\Gamma_v\left[\bar{s}_v - \frac{b^2}{s_v}\right] + 2\frac{\partial}{\partial t}\left[\sum_{v=1}^{N_v}\Gamma_v\left(\bar{s}_v - \frac{b^2}{s_v}\right)\right]. \quad (34)$$

The last term can be evaluated numerically by a finite difference scheme. For H rotor computations a third order scheme will lead to stable computation whereas a second order scheme will be stable for pitching computation. The first order scheme is unstable for any simulations including rotations.

8. Tests and perspectives

8.1. Unsteady motion of a wing profile at high Reynolds number and small angles of attack

The first series of test consider a single blade profile in unsteady pitch and heaving motion (which is important for aeroelastic coupling). The model considers a blade pitching and heaving in a sinusoidal manner with a trailing vortex sheet only. This model gives acceptable results for low angles of attacks and slightly unsteady flow. The results from (31), (32) and (34) are tested against both experimental results from Piziali [35] and analytical formulas from Theodorsen [36]. The Theodorsen formulas model the unsteady behavior of a blade and even wing aileron combination in pitch and heave by modeling the wing as a flat plate. In these motions the main parameter to represent the unsteadiness is the reduced frequency

$$k = \omega c/2V_0, \quad (35)$$

where $\omega = 2\pi f$, f is the frequency of the pitching or heaving motion, c the airfoil chord and V_0 the asymptotic wind speed or the forward translating speed of the foil. Piziali [35] made extensive series of measurements on a NACA0015 with a high Reynolds number of one million in sinusoidal pitching motion.

The main numerical parameters such as the position of the nascent vortex, the kernel vortex type and the time step do not influence much the results from the simulations. The number of vortices at the end of each simulation (around 5 to 6 cycles) is in the range of 10 000. Due to the good computational efficiency of the FMM the simulations require only a few minutes on a laptop 1.6 GHz personal computer.

The first tests consider a NACA0015 profile oscillating in pitch from 2 to 6 degrees with a reduced frequency of 0.038 (see Fig. 4) and from 1.8 to 6.2 degrees at a reduced frequency of 0.19 (see Fig. 5).

In Fig. 4 the experimental results for the lift coefficients of Piziali [35] and the analytical results of Theodorsen [36] agree particularly well whereas the present simulation agrees for the qualitative behavior but are shifted to higher lift coefficients. This can be explained as follows: Theodorsen [36] did not include all transients' effects and benefits from an underestimate nearly coinciding with viscous effects (Inviscid simulations overestimate the lift coefficient [37]). It is therefore logical that the inviscid results are shifted to higher values for the lift coefficient. In the NASA experiments [35] the viscous effects would reduce the lift from the inviscid solution. The thicker the airfoil the more the lift increases according to the inviscid theory. The results of the simulation are therefore considered to be realistic within the approximations done within the model. In Fig. 5 the same phenomenon is observed but the width of the hysteresis loop is decreased compared to the lower reduced frequencies. This is correctly modeled by the present simulation. The same shift to higher lift values is observed which is also due to the inviscid assumption. This time the underestimation in the theory [36] is obvious.

The second test considers a flat plate and a NACA0015 profile in sinusoidal heaving oscillation. The Theodorsen formulas are compared to the results of the simulation. The lift hysteresis loop fits with the Theodorsen formulas at a high reduced frequency in Fig. 6 and deviates only slightly in the NACA0015 case.

Although the full Navier–Stokes equations are far from being solved here, the ability of the model to incorporate viscous effects via a continuous release of vorticity inside a vortex particle

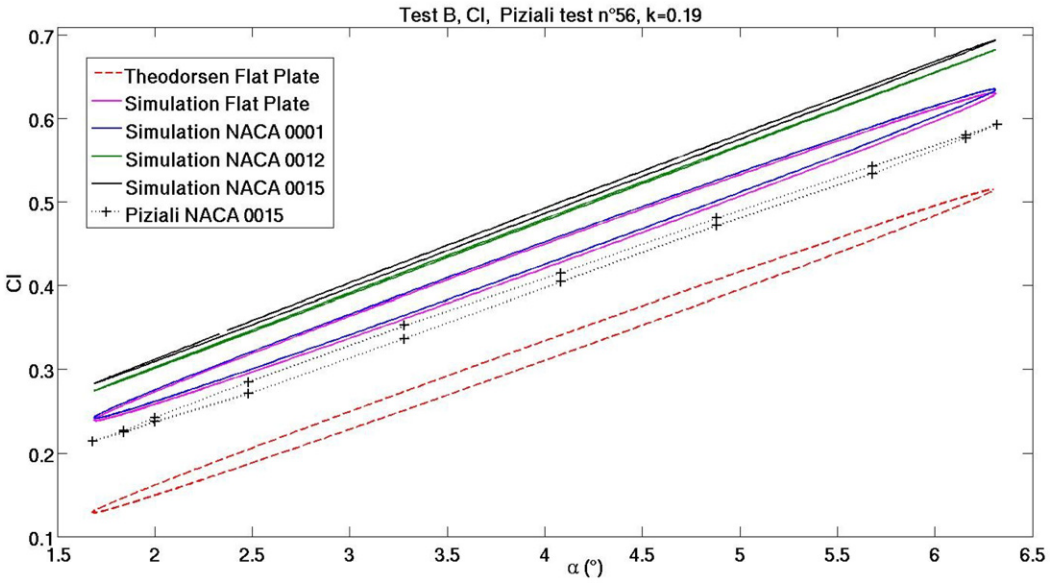

Fig. 5. Lift coefficient vs. pitch angle for different profiles in sinusoidal pitching motion with a high reduced frequency of 0.19 with a pitch from 1.8 to 6.2 degrees. (For interpretation of the references to colour in this figure legend, the reader is referred to the web version of this article.)

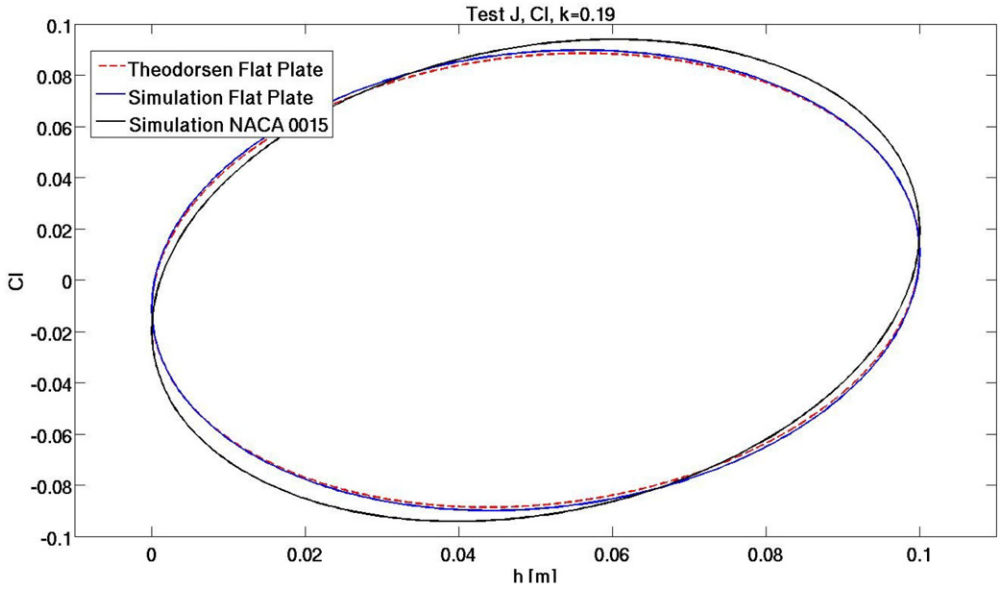

Fig. 6. Lift coefficient vs. heave position for different profiles in sinusoidal heaving motion with a high reduced frequency of 0.19 and for a heave parameter varying from 0 to 0.1. (For interpretation of the references to colour in this figure legend, the reader is referred to the web version of this article.)

method is emphasized in the following section via two numerical tests. A complete description of the numerical model used in Section 8.2 is developed in [22]. The base of the method to solve the Navier–Stokes equations is the same as the one developed in Sections 3–7 although the method developed in [22] is for multiple sections but did not considered the motion of the sections. As such the present "inviscid" part can be considered as the "inviscid" basis for an unsteady Navier–Stokes model with moving boundaries.

8.2. Perspectives: unsteady lift on a profile in stall at low (5000) to medium (33 000) Reynolds number

A FX79-w151a profile at a high angle of attack of 12 degrees and two Reynolds numbers is considered. This test has been chosen in order to compare with the unsteady lift and drag obtained from a spectral method to solve the full unsteady Navier–Stokes equations described in [38] and [39]. In this case, the numerical parameters are more important and should be chosen more carefully than in the trailing vortex sheet models. The vortices are released following the approach of Shih [40] and Subramanian [41]. The time step used is $\Delta t = 0.01$ s for the first simulation at a Reynolds number of 5000 (Figs. 7 and 8) and $\Delta t = 0.005$ s for the second at Reynolds number of 33 000 (Figs. 9 and 10). These choices are made for a unit chord and unit asymptotic incoming wind speed and correspond to the parameters used in [41] for equivalent Reynolds numbers. The number of particles after 14 and 7 s of simulation, respectively, has increased to about 200 000. The total computing time for both simulations is around 10 hours. For this large number of particles, one convection step takes around 60 s on a single processor 2.6 GHz computer. The convection step is achieved with a Runge–Kutta second order method. The diffusion is modeled via the random walk method with Strang splitting [42]. The particles are not re-ordered (no re-meshing scheme) during the whole simulation.

The first set of plots in Fig. 7 represents the vorticity shed from the FX79-w151a profile at 12 degrees of attack and a Reynolds

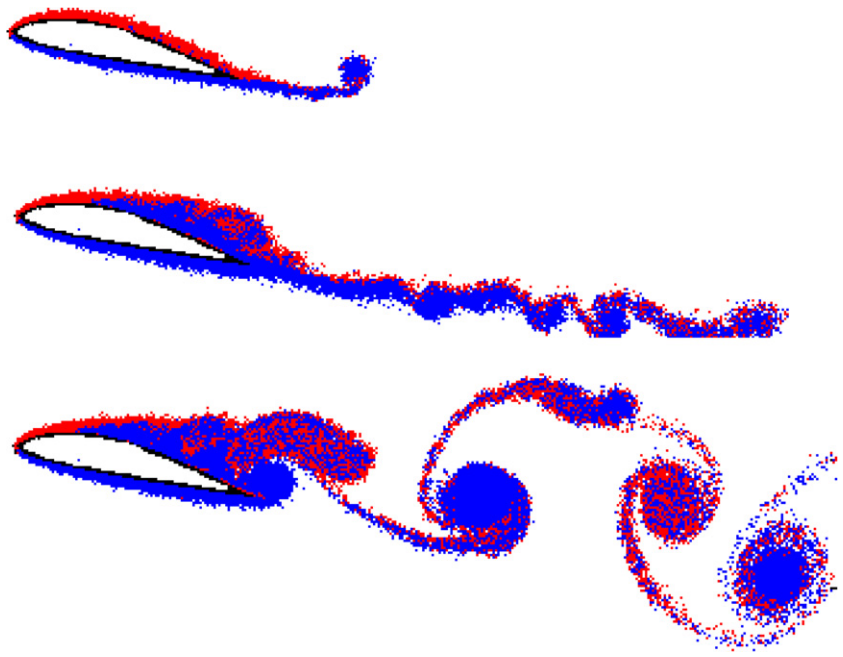

Fig. 7. Vortex trace plots of the flow past a FX79-w151a profile at a large angle of attack of 12 degrees and a low Reynolds number of 5000.

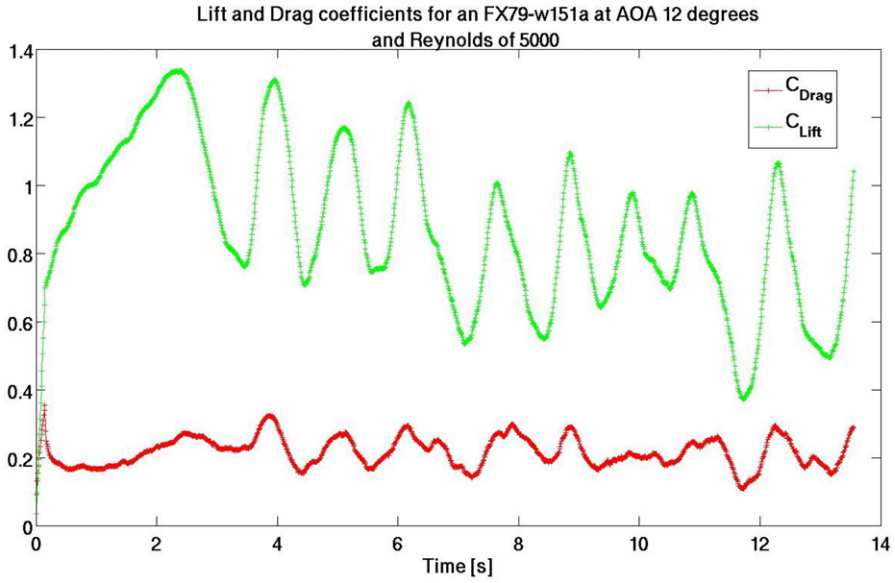

Fig. 8. Lift coefficient (green) and drag coefficient (red) against time for the flow in Fig. 9. (For interpretation of the references to colour in this figure legend, the reader is referred to the web version of this article.)

number of 5000. Clockwise vortices are colored in red and anticlockwise in blue. In Fig. 7, the start up vortex first develops and the boundary layer stays attached. Then, the boundary layer detaches at 30% of the chord length from the leading edge and interacts with trailing edge vortices to form a Karman vortex street. Although the periodic character of the flow is less obvious than in the simulations of Stoevesandt [38] using spectral methods, the mean lift and drag forces (see Fig. 8) are very similar. Moreover the Strouhal number, or natural frequency, of this profile and at this Reynolds number is identical. The flow is more chaotic in the present simulation, an effect probably due to the stochastic diffusion algorithm used. Future work will include a modified Particle Strength Exchange (PSE) scheme with automatic remeshing [41].

In Fig. 9, the vorticity for the same situation but at a higher Reynolds number of 33 000 is plotted. The boundary layer is much thinner and the characteristic size of the eddies is decreased. Moreover the vortex shedding frequency is higher and the amplitude of the oscillations smaller. This is perfectly coherent with the spectral simulations of Stoevesandt [39] both in terms of flow behavior and average lift and drag forces (see Fig. 10).

Although the agreement is good between the 2D simulations using spectral and vortex methods, the simulations in this paper are an attempt to solve complicated engineering problems with an efficient approach. At these Reynolds numbers 3D effects come into play [43]. Therefore these simulations cannot give a detailed agreement with experimental data although recent work [44] shows that 2D DNS simulations can present the correct flow picture up to Reynolds of 60 000. Anyhow, the spectral method of Stoevesandt [38] needs several days of CPU time on a cluster of computers compared to the CPU time of hours (on a PC) needed for the vortex method. Both results agree qualitatively. Regarding

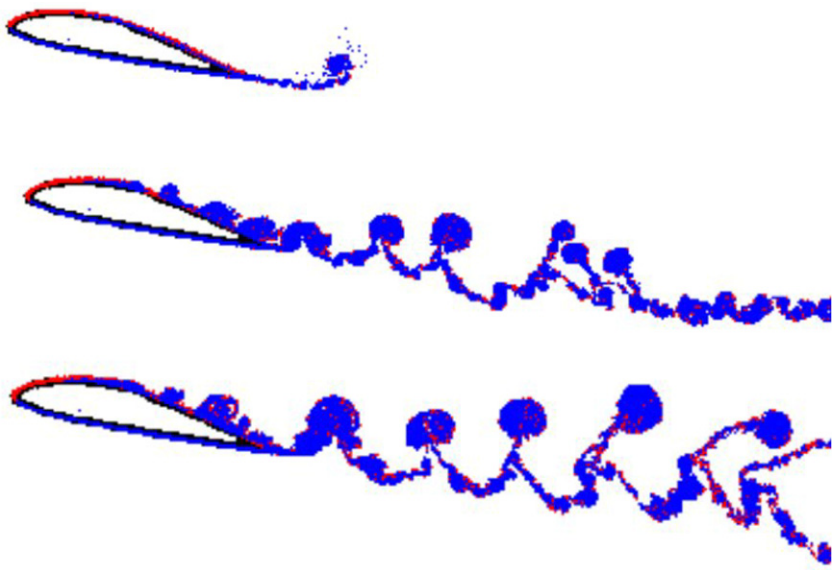

Fig. 9. Vortex trace plot of the flow past a FX79-w151a profile at a high angle of attack of 12 degrees and a Reynolds number of 33 000.

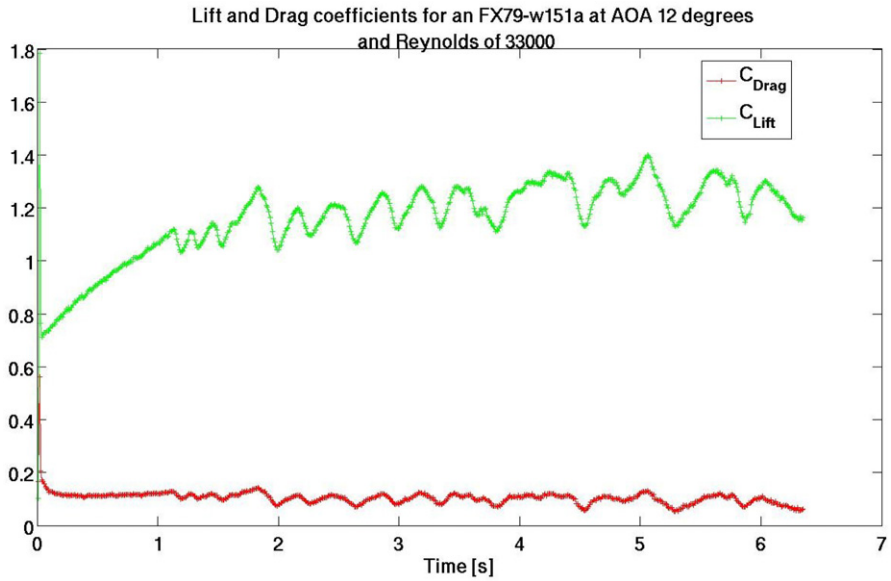

Fig. 10. Lift coefficient (green) and drag coefficient (red) against time for the flow in Fig. 11. (For interpretation of the references to colour in this figure legend, the reader is referred to the web version of this article.)

the similar results, the improvement in CPU time shows a great advantage of the presented model.

8.3. H rotor flows

In all the following computations, a single bladed H rotor with a chord to radius ratio of 0.25 [9] and operating at a tip speed ratio of 5 is considered. Concerning the numerical computation, each revolution of the rotor represents 200 to 400 time steps and the results are considered for the 6th revolution. The convection of vortices is carried out with direct summation for this low number of vortices and the time stepping scheme uses the forward Euler method, as the Runge–Kutta method did not affect the results significantly. All computations lasted for 1–2 minutes on a 1.6 GHz laptop computer. This can be compared to hours of CPU time used in Ponta [11].

Two important parameters in H rotor aerodynamics, the tangential and normal forces coefficients, are considered. The tangential force is proportional to the torque coefficient produced by one blade (up to pitching moment corrections). The normal force coefficients are mainly important for fatigue issues on the carrying arms and junctions, and bending of the blades. The normal and tangential forces coefficient are defined as

$$C_T = \frac{T}{\frac{\rho}{2} V_0^2 c}, \tag{36}$$

and

$$C_N = \frac{N}{\frac{\rho}{2} V_0^2 c}, \tag{37}$$

where T and N are the normal and tangential force (with respect to the circle tangent at the attachment point) expressed in Newton, ρ the fluid mass per volume, V_0 the asymptotic wind or current speed and c the chord of the foil. T and N are directly given by Eq. (31).

In Fig. 11 the normal and tangential forces analogous to Oler [9] experimental and numerical study with one NACA0015 pro-

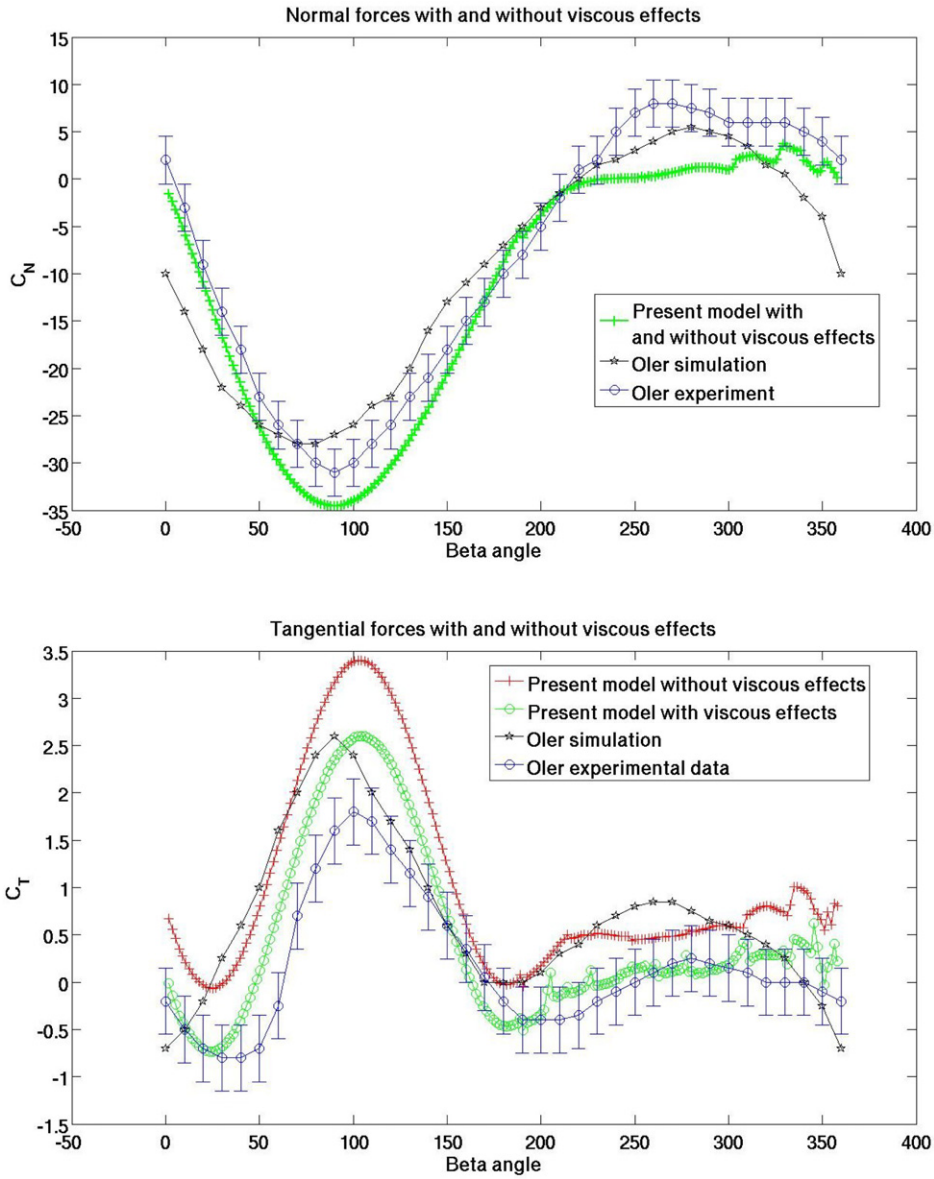

Fig. 11. Normal and tangential force coefficients against angular position for an H rotor with Oler's [9] experiment parameters. (For interpretation of the references to colour in this figure legend, the reader is referred to the web version of this article.)

file attached at the mid chord ($x_0 = 0$) are plotted against the beta position. The non-viscous simulation includes the unsteady motion of the blade plus one trailing vortex sheet whereas the viscous simulation also assumes one vortex sheet but includes in the drag calculations an integral boundary layer representation using a modified Thwaites' and Head's method [45]. This integral boundary layer representation has only been used for this test. It is similar to the one used in Oler [9] and applied to the same problem. The Reynolds number in Oler's experiments [9] is 40 000 and is outside the assumption of those theories but a qualitative agreement can be expected. The viscous influence is to lower the tangential force, as compared to the raw experimental data of Oler [9]. The results from the viscous and inviscid simulation qualitatively agree whereas the viscous simulation fits better (28% error in the tangential force coefficient in Fig. 11 and 16% error for both simulations in the normal forces). The discrepancies between the viscous simulation and the experimental results for the normal force are first due to the low Reynolds number considered, which not only increases the drag but also significantly decreases the lift. Hence the power extracted from the upwind pass is too high and the speed is too much reduced in the downwind pass inducing simulated normal forces that are too low. Secondly, the aspect ratio used in Oler experiment [9] is low and might suggest a 3D influence. Other authors [11,12] have not compared their simulation to this very hard case but instead compared with measurements of Klimas [46] with a two bladed H rotor at lower chord to radius ratio of 0.15. They found a general good agreement with their simulation. Preliminary results from Österberg [20] using a generalized version of the present simulation show similar agreements as Ponta [11] and Wang [12]. Generally, the results from other recent simulations [11], shows a similar agreement but at a much higher CPU time and the results of the vortex method in Fig. 11 of Oler [9] are poorer.

The inviscid simulation is expected to provide a realistic model for higher Reynolds numbers. For instance, a typical Reynolds number value is about 300 000 for a kW range turbine. For these reasons only the results of the inviscid simulation will be taken into account for now in Figs. 12–14.

In Fig. 12 also using the Oler experiments parameters, the effect of the fixed pitch angle on the normal forces and on the

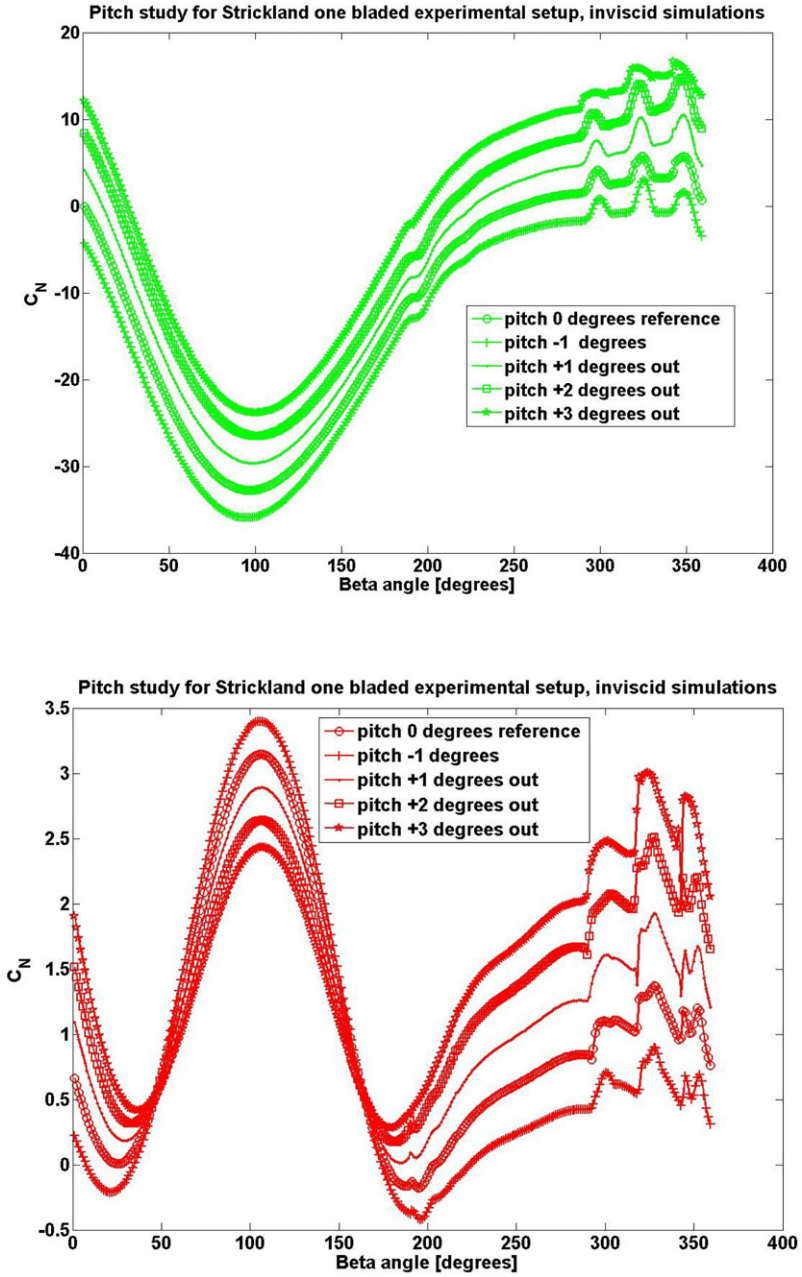

Fig. 12. Pitch angle influence on the normal (green) and tangential force coefficient (red) against angular position for an H rotor with Oler [9] experiment parameters using the inviscid simulation.

tangential forces is investigated. Paraschivoiu [3] includes experimental studies on the fixed pitch effect on straight bladed turbine performance and noticed a slight increase in averaged power when the leading edge of the foils were pitched out of the circle (for counterclockwise rotation). Although the averages of normal and tangential forces are quite similar, the amplitudes on the upwind and downwind part of the turbine show significant variations. For instance, a 3 degrees pitched turbine in this configuration (chord to radius ratio of 0.25) will absorb most of the power in the downwind pass. Pitching the foil by a few degrees decreases the local angle of attack in the upwind pass and increases it in the downwind pass which is made wider by the flow expansion. This can explain the slightly higher averaged power produced with positive fixed pitch configuration. Considering fatigue effects, it is important to balance as much as possible the sum of the normal forces plus the centrifugal forces and in a smaller proportion the tangential forces between the upwind and downwind position. This can lead to lower bending stresses amplitudes but also to decrease the fluctuations in the torque produced. Fig. 12 shows that the pitching of the blade can be an interesting parameter for the H rotor designer. Moreover, the instantaneous forces can be significantly affected by a pitch angle error.

In Fig. 13 the effect of moving the attachment point is studied. From the previous pitch study (see Fig. 12) a similar trend is noticed: moving the attachment point forward increases the energy capture in the upwind pass and decreases it in the downwind pass. The pitch angle and attachment point variations are indeed equivalent via basic trigonometry. Moreover, an important difference between Darrieus rotors and H rotors is that Darrieus turbines typically have a mid chord attachment point, whereas H rotors have a quarter chord attachment point to minimize the aerodynamic

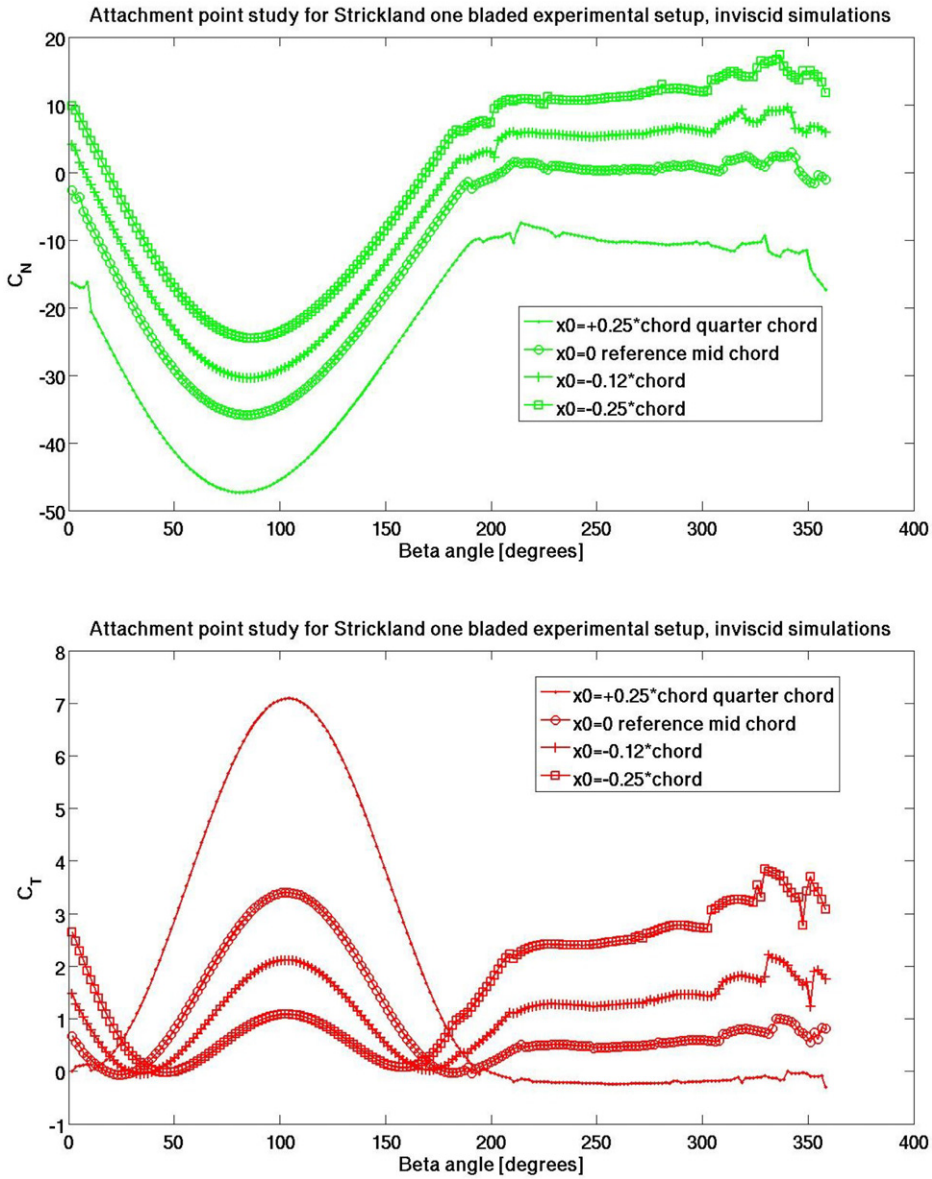

Fig. 13. Attachment point influence on the normal (green) and tangential force coefficient (red) against angular position for an H rotor with Oler [9] experiment parameters using the inviscid simulation.

moment at the strut blade junction. At this high chord to radius ratio of 0.25, the difference in instantaneous normal and tangential forces is striking.

In Fig. 14 the effect of the camber and position of maximum of camber along the chord-line of the blade profile for the Oler base experiment is investigated. Whereas pitch and attachment point variations show completely different results in terms of force coefficients, the camber seems to be a parameter of secondary influence. Here again there is no win-win strategy: an increase in the upwind pass decreases the tangential force in the downwind pass. The NACA2515 seems to be a good compromise for this configuration. Even the influence of moving the maximum of camber position can be studied and shows slight differences between the NACA1215 and the NACA1715. It has to be stressed that camber influence might be different in practice due to eventual viscous effects.

In Fig. 15 the wake or trajectory of the trailing edge vortex sheet has been pictured for the experimental setup of Klimas [46] with one blade. The wind is blowing from left to right. Fig. 15 shows analogous trends as the theoretical results of Ponta [11], Wang [12] and the experimental results of Klimas [46]. A stable vortex street forms at the upper and lower extreme points where most of the vorticity is shed.

Although the results here given are promising, the theory developed needs further improvements to be completed. The main aspects to be incorporated in a complete model are the eventual action of the viscous flow on the inviscid flow, dynamic stall effects and 3D effects. The aeroelastic coupling is also of important practical interest and can be derived from the present model using strips of this 2D model which is a common approach to study instabilities along marine cables [47].

9. Conclusion

An analytical model for the 2D unsteady flow around an arbitrary profile in arbitrary motion has been developed. The model uses conformal mapping techniques to allow for fast analytical calculations: the solution is derived for a single circle and generalized to arbitrary geometries via conformal mapping techniques. The model is self consistent with no added parameter adjustments.

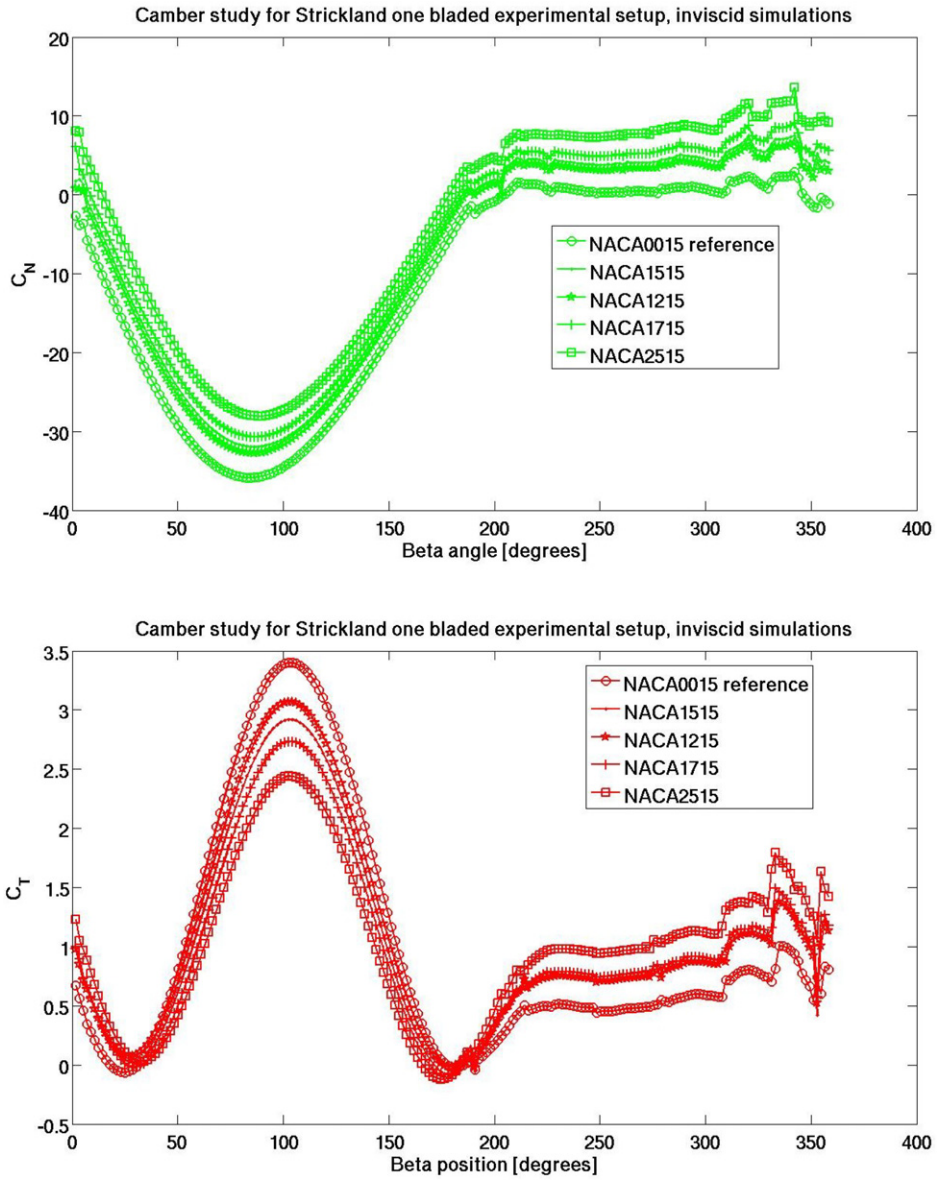

Fig. 14. Camber and position of camber influence on the normal (green) and tangential force coefficient (red) against angular position for an H rotor with Oler [9] experiment parameters using the inviscid simulation.

Discrete point vortices describe the complicated flow structure experienced by the moving blade. Arbitrary shapes of the profile can be modeled. The strengths of the model are that it is physically transparent and easy to apply in an effective and fast way. The use of analytical formulas shortens and clarifies the presentation, computation and computation benchmarking. The results from the model agree well with experiments so far conducted. It describes qualitative behavior, with the same accuracy, in much shorter computation time than previous models. That makes it straight forward to apply for aeroelastic calculations to be treated in a subsequent paper. The model is well suited as a design tool for vertical axis turbines. Further developments will allow for a generalization of the theory to include several objects and to design multi-bladed turbines.

Acknowledgements

Mathias Bouquerel is acknowledged for performing the tests comparing Theodorsen theories and Piziali's experiments. David Österberg is acknowledged for his implementation of the present theory applied to N bodies. Michèle Larcheveque (Paris VI) and Bodil Branner (DTU) are thanked for their excellent courses in complex number analysis. The Swedish Energy Agency (STEM) through the Centre for Renewable Energy conversion, the Swedish agency for innovations systems (VINNOVA) and the Swedish National Graduate School in Mathematics and Computing (FMB) have partly financed this study. Anders Goude is acknowledged to have checked the analytical formulas contained in this paper.

Appendix A

Analytical expressions for the complex potential solution to the problem stated in Section 4

$$G_{A,1} = (\overline{H+\sigma})c_1 + (H+\sigma)b + d_1, \tag{A.1}$$

$$G_{A,k>1} = (\overline{H+\sigma})c_k + c_{k-1}b + d_k, \tag{A.2}$$

with

$$d_k = \sum_{j=1}^{\infty} c_{j+k}\overline{c_j}, \tag{A.3}$$

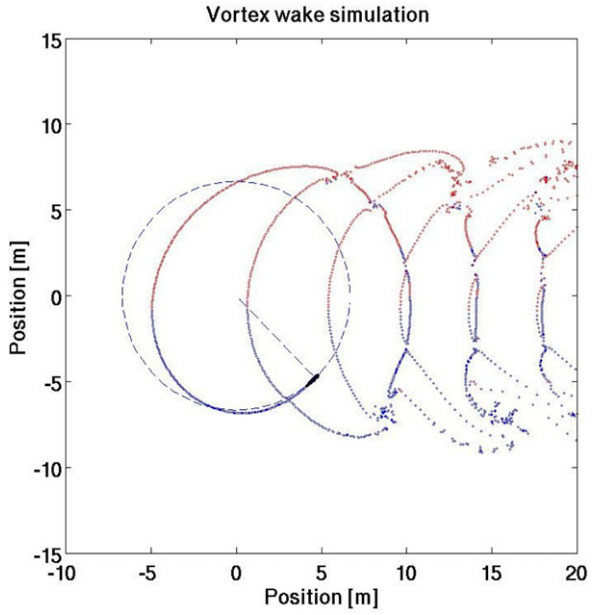

Fig. 15. Vortex trace plot of the flow past an H rotor with Klimas [46] experimental setup and simulation.

$$H = iae^{i\delta} + x_0. \tag{A.4}$$

The coefficients $\{G_{B,k}\}_{k\in N}$ for the rotation along δ can easily be derived by noting that they correspond to $\{G_{A,k}\}_{k\in N}$ with $a = 0$ and $\beta = 0$. Therefore with $\hat{H} = x_0$ is obtained:

$$G_{B,1} = (\overline{x_0 + \sigma})c_1 + (x_0 + \sigma)b + d_1, \tag{A.5}$$

$$G_{B,k>1} = (\overline{x_0 + \sigma})c_k + c_{k-1}b + d_k, \tag{A.6}$$

where the $\{d_k\}_{k\in N}$ are identical to the terms appearing in the expressions for $\{G_{A,k}\}_{k\in N}$.

The two sets of coefficients corresponding to the translations $\{G_{C,k}\}_{k\in N}$ and $\{G_{D,k}\}_{k\in N}$ are given by:

$$G_{C,1} = e^{-i\delta}c_1 + be^{i\delta}, \tag{A.7}$$

$$G_{C,k>1} = c_k e^{-i\delta}. \tag{A.8}$$

And finally

$$G_{D,1} = c_1 - b, \tag{A.9}$$

$$G_{D,k>1} = c_k. \tag{A.10}$$

Appendix B. Calculation of forces

It is possible to calculate the total forces from the complex potential via

$$X - iY = \frac{i\rho}{2}\left[\oint_C \left(\frac{dF}{dz}\right)^2 dz - \oint_C \bar{V}_{z/z3z}\, dF - \oint_C \bar{V}_{z/z3z}\, d\bar{F} + \oint_C \frac{\partial F}{\partial t}\, d\bar{z} + \oint_C \frac{\overline{\partial F}}{\partial t}\, d\bar{z}\right]. \tag{B.1}$$

Where $V_{z/z3z}$ is the velocity of all points moving in the z_3 frame fixed in the z frame expressed in the z frame as

$$V_{z/z3inz} = i\dot{\beta}z_3 e^{-i\beta}e^{i\delta} + \dot{x}_0 - i\dot{\delta}z_1 e^{i\delta} + i\dot{a}e^{i\delta}. \tag{B.2}$$

Note that the terms containing time will have a special treatment afterwards to take into account the nascent vortices.

If we define

$$B = \oint_C \left(\frac{dF}{dz}\right)^2 dz = \oint_C \left(\frac{dF}{ds}\right)^2 \frac{1}{f'(s)}\, ds, \tag{B.3}$$

$$C = -\oint_C \bar{V}_{entz}\, dF - \oint_C \bar{V}_{entz}\, d\bar{F}, \tag{B.4}$$

$$D = \oint_C \frac{\partial F}{\partial t}\, d\bar{z} + \oint_C \frac{\overline{\partial F}}{\partial t}\, d\bar{z}. \tag{B.5}$$

We find that the exact formula for the forces from the fluid onto the wing will be

$$X - iY = \frac{i\rho}{2}[B + C + D], \tag{B.6}$$

with

$$B = 2\sum_{\nu=1}^{N_\nu} \Gamma_\nu \frac{d\bar{z}_\nu}{dt}, \tag{B.7}$$

$$C/2 = -\bar{V}_{z/z3inz0}\sum_{\nu=1}^{N_\nu}\Gamma_\nu - 2(\dot{\beta} - \dot{\delta})\pi\left(V_0 e^{i(-\alpha+\beta-\delta)}b^2 + \bar{G}_1 b - V_0 e^{-i(-\alpha+\beta-\delta)}\bar{c}_1 b\right) + i(\dot{\beta} - \dot{\delta})\sum_{\nu=1}^{N_\nu}\Gamma_\nu\left[\bar{z}_\nu - \bar{s}_\nu + \frac{b^2}{s_\nu}\right] - (\dot{\beta} - \dot{\delta})\bar{V}_{z/z3inz0}A + i(\dot{\beta} - \dot{\delta})^2\frac{2A}{3}\bar{\zeta}, \tag{B.8}$$

$$D = -\frac{4A}{3}\bar{\zeta}\left[\ddot{\delta} - \ddot{\beta}\right] - 2iAA_{z/z3inz} - 2\sum_{\nu=1}^{N_\nu}\Gamma_\nu\left[\frac{\partial\bar{s}_\nu}{\partial t}\frac{d\bar{z}_\nu}{d\bar{s}_\nu} - \frac{\partial\bar{s}_\nu}{\partial t} + \frac{\partial}{\partial t}\left(\frac{b^2}{s_\nu}\right)\right] + 4i\pi b\left\{\bar{c}_1\left[\frac{\partial V_0}{\partial t}e^{-i(-\alpha+\beta-\delta)} - V_0 i(-\dot{\alpha} + \dot{\beta} - \dot{\delta})e^{-i(-\alpha+\beta-\delta)}\right] - \bar{\dot{D}}_1\right\}, \tag{B.9}$$

where A is the area of the profile, ζ the complex position of the center of moment, $V_{z/z3inz0}$ is defined as the constant part of

$$V_{z/z3inz} = V_{z/z3inz0} + i(\dot{\beta} - \dot{\delta})z, \tag{B.10}$$

and $A_{z/z3inz}$ is given as the acceleration:

$$A_{z/z3inz} = \ddot{\beta}\left(-ix_0 - ae^{-i\delta}\right) + \dot{\beta}\left(-i\dot{x}_0 - \dot{a}e^{-i\delta}\right) + i\dot{\delta}\dot{\beta}ae^{-i\delta} + i\ddot{\delta}x_0 + \dot{\delta}\left(i\dot{x}_0 - \dot{a}e^{-i\delta}\right) - i\ddot{a}e^{-i\delta} + \ddot{x}_0. \tag{B.11}$$

Finally D_1 is such that

$$\dot{D}_1 = \frac{\partial V_0}{\partial t}e^{-i(-\alpha+\beta-\delta)}b - V_0 i(-\dot{\alpha} + \dot{\beta} - \dot{\delta})e^{-i(-\alpha+\beta-\delta)}b + \dot{G}_1,$$
$$\dot{D}_k = \dot{G}_k. \tag{B.12}$$

Grouping first the other terms and then vortex dependent ones

$$X - iY = \frac{i\rho}{2}[E + I]. \tag{B.13}$$

References

[1] G.J.M. Darrieus, Turbine having its rotating shaft transverse to the flow of the current, US Patent no. 1.835.018, 1931.
[2] S. Eriksson, H. Bernhoff, M. Leijon, Evaluation of different turbine concepts for wind power, Renewable and Sustainable Energy Reviews 12 (5) (June 2008) 1419–1434.
[3] I. Paraschivoiu, Wind Turbine Design with Emphasis on Darrieus Concept, Polytechnic Int. Press, 2002.
[4] P.W. Carlin, A.S. Laxson, E. Muljadi, The History and State of the Art of Variable-Speed Wind Turbine Technology, Technical Report, NREL/TP-500-28607, 2001.

[5] C.A. Morgan, P. Gardner, I.D. Mays, M.B. Anderson, The demonstration of a stall regulated 100 KW vertical axis wind turbine“ EWEC, 645, 1989.
[6] J.M. Anderson, K. Streitlien, D.S. Barrett, M.S. Triantafyllou, Flapping foils of high propulsive efficiency, Journal of Fluid Mechanics 360 (1998) 41–72.
[7] P.G. Migliore, W.P. Wolfe, J.B. Fanucci, Flow curvature effects on Darrieus turbine blade aerodynamics, Journal of Energy 4 (2) (1980) 49–55.
[8] G.F. Homicz, Numerical simulation of VAWT stochastic aerodynamics loads produced by atmospheric turbulence: VAWT-SAL Code, SANDIA REPORT, SAND91-1124 UC-261, September 1991.
[9] J.W. Oler, J.H. Strickland, B.J. Im, G.H. Graham, Dynamic stall regulation of the Darrieus turbine, SANDIA REPORT, SAND83-7029 UC-261, August 1983.
[10] R.E. Wilson, P.B. S Lissaman, M. James, W.R. McKie, Aerodynamic loads on a Darrieus rotor blade, Journal of Fluids Engineering 105 (March 1983) 53–58.
[11] F.L. Ponta, P.M. Jacovkis, A vortex model for Darrieus turbine using finite element techniques, Renewable Energy 24 (1) (September 2001) 1–18.
[12] L.B. Wang, L. Zhang, N.D. Zeng, A potential flow 2D vortex panel model, Applications to vertical axis straight blade tidal turbine, Energy Conversion and Management 48 (2) (February 2007) 454–461.
[13] I.S. Hwang, S.Y. Min, S.J. Kim, Multidisciplinary optimal design of cyclocopter blade system, in: 46th AIAA/ASME/ASCE/AHS/ASC Structures, Structural Dynamics & Materials Conference, Austin, TX, 18–21 April 2005, AIAA 2005-22.
[14] M.O.L. Hansen, D.N. Sørensen, CFD model for vertical axis wind turbine, in: Proceedings of the 2001 European Wind Energy Conference and Exhibition, WIP-Renewable Energies, Munich, 2001, pp. 485–487.
[15] J. Zhang, Numerical modelling of Vertical Axis Wind Turbine (VAWT), Master thesis, Technical University of Denmark, Dept Mechanical Engineering, 2004.
[16] A. Zervos, S. Desspipris, N. Athanassiadis, Optimization of the performance of the variable pitch vertical axis wind turbine, EWEC, 1984.
[17] G. Couchet, Mouvement plan d'un fluide en présence d'un profil mobile, Memorial des Sciences Mathematiques, vol. 135, Gauthier-Villars, Paris, 1956.
[18] L. Zannetti, F. Gallizio, G. Ottino, Vortex capturing vertical axis wind turbine, in: The Science of Making Torque from Wind, Journal of Physics: Conference Series 75 (2007) 012029, doi:10.1088/1742-6596/75/1/012029. IOP Publishing.
[19] J. Carrier, L. Greengard, V. Rokhlin, A fast adaptative multipole algorithm for particle simulations, SIAM Journal of Scientific and Statistical Computing (July 1998).
[20] D. Österberg, Master thesis, Dept of Engineering Science, Uppsala University, 2008.
[21] S.G. Krantz, in: Handbook of Complex Variables, Birkhäuser, Boston, MA, 1999, pp. 86–87.
[22] P. Deglaire, O. Ågren, H. Bernhoff, M. Leijon, Conformal mapping and efficient boundary element method without boundary elements for fast vortex particle simulations, European Journal of Mechanics B/Fluids 27 (2) (March–April 2008) 150–176.
[23] D.C. Ives, A modern look at conformal mapping including multiply connected regions, AIAA Journal 14 (1976) 1006–1011.
[24] E.B. Saff, A.D. Snider, Fundamentals of Complex Analysis with Applications to Engineering and Science, third ed., Prentice Hall, Upper Saddle River, NJ, ISBN 0-13-907874-6, 2003.
[25] K. Streitlien, M.S. Triantafyllou, Force and moment on a Joukowski profile in the Presence of point vortices, AIAA Journal 33 (4) (April 1995).
[26] R.R. Clements, An inviscid model of two dimensional vortex shedding, Journal of Fluid Mechanics 57 (2) (1973) 321–336.
[27] L. Greengard, V. Rokhlin, A fast algorithm for particle simulations, Journal of Computational Physics 73 (1987) 325–348.
[28] W.D. Elliott, J.A. Board, Fast Fourier transform accelerated fast multipole algorithm, SIAM Journal of Scientific Computing 17 (2) (1996) 398–415.
[29] L. Greengard, V. Rokhlin, A new version of the fast multipole method for the Laplace equation in three dimensions, Acta Numerica 6 (1997) 229–269.
[30] H. Cheng, L. Greengard, V. Rokhlin, A fast adaptive multipole algorithm in three dimensions, Journal of Computational Physics 155 (1999) 468–498.
[31] M.S. Warren, J.K. Salmon, A fast tree code for many-body problems, in: N.G. Cooper (Ed.), Los Alamos Science, vol. 22, Los Alamos National Laboratory, Los Alamos, NM, 1994, pp. 88–97.
[32] Basic Linear Algebra Subprograms, http://www.netlib.org/blas/.
[33] FMM code http://user.it.uu.se/~stefane.
[34] L.M. Milne-Thomson, Theoretical Hydrodynamics, Macmillan Co., New York, 1967.
[35] R.A. Piziali, 2D and 3D Oscillating wing aerodynamic for a range of angles of attack including stall, NASA TM 4632, Technical report 94-A-011, September 1994.
[36] T. Theodorsen, General theory of aerodynamic instability and the mechanism of flutter, NACA-ARR-1935, NACA-TR-496, 1949.
[37] M. Drela, XFOIL: An Analysis and Design System for Low Reynolds Number Airfoils, in: Lecture Notes in Engineering Low Reynolds Number Aerodynamics, vol. 54, Springer-Verlag, New York, 1989.
[38] B. Stoevesandt, A. Shishkin, J. Peinke, C. Wagner, Computational simulation of the turbulent flow around an airfoil using spectral/HP method, presented at the EWEC 2007, Milan, 2007.
[39] B. Stoevesandt, A. Shishkin, J. Peinke, C. Wagner, Direct numerical simulation of the turbulent flow around an airfoil using spectral/HP method, in: European Conference on Computational Fluid Dynamics, ECCOMAS CFD 2006, 2006.
[40] C. Shih, L. Lourenco, L. Van Dommelen, A. Krothapalli, Unsteady flow past an airfoil pitching at a constant rate, AIAA Journal 30 (1992) 1153–1161.
[41] S. Subramaniam, A new mesh-free vortex method, PhD thesis, Florida State University, 1996.
[42] P. Ramachandran, Development and study of a high-resolution two-dimensional random vortex method, Ph.D. Thesis, Indian Institute of Technology, Madras, India, June 2004.
[43] M. Braza, R. Perrin, Y. Hoarau, Turbulence properties in the cylinder wake at high Reynolds number, Conférence plénière invitée, International Symposium BBVIV4, “Bluff Body, Wakes and Vortex Induced Vibrations-4”, Santorini, June 2005.
[44] Y. Elimelech, R. Arieli, G. Iosilevskii, Flow over NACA0009 and Eppler 61 airfoils at low Reynolds number of 5000 to 60,000, AIAA Journal 45 (10) (October 2007).
[45] J. Moran, An Introduction to Theoretical and Computational Aerodynamics, Wiley, New York, 1984.
[46] P.C. Klimas, Darrieus rotor aerodynamics, in: Biennial Wind Energy Conference and Workshop, 5th, Washington, DC, Oct. 5–7, 1981, ASME, Transactions, Journal of Solar Energy Engineering 104 (May 1982) 102–105.
[47] B. Molin, Hydrodynamique des structures offshore, Editions Technip, 2002.